Translational Stroke Research (2018) 9:643–653
https://doi.org/10.1007/s12975-018-0615-1

ORIGINAL ARTICLE

Focal Ischaemic Infarcts Expand Faster in Cerebellar Cortex than Cerebral Cortex in a Mouse Photothrombotic Stroke Model

Nagarajesh Gorlamandala[1] · Jasneet Parmar[1] · Amanda J. Craig[1] · John M. Power[1] · Andrew J. Moorhouse[2] · Arun V. Krishnan[1,3,4] · Gary D. Housley[1]

Received: 20 December 2017 / Revised: 2 February 2018 / Accepted: 4 February 2018 / Published online: 17 February 2018

Abstract

It is generally accepted that the cerebellum is particularly vulnerable to ischaemic injury, and this may contribute to the high mortality arising from posterior circulation strokes. However, this has not been systematically examined in an animal model. This study compared the development and resolution of matched photothrombotic microvascular infarcts in the cerebellar and cerebral cortices in adult 129/SvEv mice of both sexes. The photothrombotic lesions were made using tail vein injection of Rose Bengal with a 532 nm laser projected onto a 2 mm diameter aperture over the target region of the brain (with skull thinning). Infarct size was then imaged histologically following 2 h to 30-day survival using serial reconstruction of haematoxylin and eosin stained cryosections. This was complemented with immunohistochemistry for neuron and glial markers. At 2 h post-injury, the cerebellar infarct volume averaged ~ 2.7 times that of the cerebral cortex infarcts. Infarct volume reached maximum in the cerebellum in a quarter of the time (24 h) taken in the cerebral cortex (4 days). Remodelling resolved the infarcts within a month, leaving significantly larger residual injury volume in the cerebellum. The death of neurons in the core lesion at 2 h was confirmed by NeuN and Calbindin immunofluorescence, alongside activation of astrocytes and microglia. The latter persisted in the region within and surrounding the residual infarct at 30 days. This comparison of acute focal ischaemic injuries in cerebellar and cerebral cortices provides direct confirmation of exacerbation of neuropathology and faster kinetics in the cerebellum.

Keywords Ischaemic brain injury · Penumbra · Brain remodelling · Astrocytes · Microglia · Purkinje neurons

Introduction

Focal ischaemic brain injury remains one of the leading causes of mortality and morbidity in the world. Thrombolytic therapy and endovascular clot retrieval are the only approved treatments that aim to restore vascular patency following an ischaemic stroke, but are limited in administration and effectiveness [1–4]. There is broad evidence that the cerebellum is

Nagarajesh Gorlamandala and Jasneet Parmar joint first authorship reflect equal contributions

✉ Gary D. Housley
g.housley@unsw.edu.au

Nagarajesh Gorlamandala
n.gorlamandala@unsw.edu.au

Jasneet Parmar
j.parmar@unsw.edu.au

Amanda J. Craig
Amanda.Craig@health.gov.au

John M. Power
john.power@unsw.edu.au

Andrew J. Moorhouse
A.Moorhouse@unsw.edu.au

Arun V. Krishnan
arun.krishnan@unsw.edu.au

[1] Translational Neuroscience Facility, Department of Physiology, School of Medical Sciences, UNSW Sydney, Sydney, NSW 2052, Australia

[2] Cellular and Systems Physiology, Department of Physiology, School of Medical Sciences, UNSW Sydney, Sydney, NSW 2052, Australia

[3] Prince of Wales Clinical School, UNSW Sydney, Sydney, NSW 2052, Australia

[4] Prince of Wales Clinical School, UNSW Sydney, Barker Street, Randwick, NSW 2031, Australia

more vulnerable to ischaemic excitotoxic injury than other regions of the brain, as it shows a more rapid progression of degeneration following global ischaemia [5, 6] and traumatic brain injury [7, 8]. Moreover, the mortality rate following a cerebellar infarction is greater than an infarct in any other brain region [9, 10]. Currently, the most widely used small animal models of focal ischaemia are directed to middle cerebral artery occlusion (MCAO) via permanent or temporary obstruction using endovascular suture or a thread inserted via the carotid artery [11, 12], or by inducing thromboembolic ischaemia, for example, by injecting thrombin directly into the middle cerebral artery [13, 14]. Local injections of endothelin-1 and photothrombotic lesions following injection of a photosensitising dye into the venous circulation have also been used to study acute focal ischaemic brain injury [15–17]. The endothelin-1 model provides versatility with regard to brain region, but has inherent variability [18, 19]. The photothrombotic lesion model generates highly reproducible lesions with low animal mortality rates when targeting cerebral cortex in rodents [20–23]. This involves a systemic administration of the photosensitive dye Rose Bengal, followed by irradiation of the exposed skull with green wavelength light [17]. The coupling of the light and the dye in the vessels generate oxygen-free radicals causing peroxidation in the endothelial cell membrane leading to platelet aggregation and thrombus formation, thus occluding blood supply to the targeted brain region [16, 17, 20]. All these approaches have enabled characterisation of the long-term progression of ischaemic brain injury in the cerebral cortex, including loss of neurons and associated glial responses, and this careful mapping of the ischaemic sequelae provides the basis for addressing the complexities of the underlying biochemical and immunological processes triggered by the acute focal injury.

Despite the prevalence and severity of posterior circulation strokes, preclinical models for characterising cerebellar ischaemic brain injury have been limited to global ischaemia, injection of autologous clots in the vertebral artery [24] or microsphere-induced embolisms via the internal carotid artery [25], which are highly invasive and lack spatiotemporal confinement. To address the question of whether the cerebellar cortical tissue has differing vulnerability to ischaemic brain injury than cerebral cortex, we adapted the photothrombotic lesion model of focal ischaemia to target both the posterior circulation of the brain and the cerebral cortex, with identical primary lesions. By injecting Rose Bengal dye via the tail vein and then delivering a consistent flux of green light illumination to either the cerebral cortex or the cerebellar cortex, we were able to achieve highly reproducible and equivalent primary infarcts in both brain regions, thereby enabling a direct comparison of the subsequent injury responses.

Materials and Methods

All experiments were approved by the UNSW Sydney Animal Care and Ethics Committee. The study utilised mice (129/SvEv strain) aged 5 to 9 weeks, both males and females, weighing 18–25 g, maintained on a 12-h light/dark cycle and fed ad libitum. This reflects early breeding age animals, where the requirement for thinning of the skull to achieve optimal photo-illumination was minimal. Thus, the possibility for mechanical trauma activating microglia was reduced, and the consistency of delivery of photo-illumination to the two regions was maximised, as shown in Fig. 1. The mice were randomly assigned to infarct target region and post-infarct time point. The photothrombotic lesions were randomised, but the experimenters were not blinded for the tissue processing. The lesion volume measurements were randomly double scored by multiple investigators.

Induction of Photothrombotic Lesion

Anaesthesia was induced in the mice using 3% isoflurane with O_2 and maintained at 1.25% isoflurane for the duration of the surgery. Heart rate and oxygen saturation were monitored throughout the surgery, and the body temperature was clamped at 37 ± 0.5 °C (Physio Suite, Able Scientific, Australia). The hair over the skull was shaved and the skin sterilised with two alternative swabs of iodine solution and 70% (weight/volume) ethanol. Local anaesthetic, Lignocaine (0.15 mg/kg), was subcutaneously injected at the site of incision. Analgesia, Temgesic (Buprenorphine; 0.15 mg/kg), was administered prior to the incision. Mice underwent cranial thinning [26] over the midline of cerebral cortex (centred 2 mm anterior to the lambda point), using a manual micromotor drill (Volvere Vmax, NSK Nakanishi Inc., Japan) until translucent. Critical to the experimental design, a dark PVC mask with a 2 mm diameter aperture was placed over the thinned cranium to restrict the laser illumination (Fig. 1a). A separate cohort of animals was used for lesions in the cerebellum, which underwent cranial thinning 2 mm posterior to the lambda point to target the cerebellar vermis (Fig. 1b). Rose Bengal dye (tetrachlorotetraiodofluorscein; Sigma-Aldrich, USA; 50 mg/kg, at 1% volume/body weight in normal saline) was injected via the tail vein, followed by immediate irradiation of the cerebrum or cerebellar target region of the brain surface with green (532 nm) laser light (~ 3 mW, 6 min) using a targeting frame. The surgical site was then sutured, and the animal was allowed to recover under O_2, with monitoring of body temperature until conscious and walking around. Animals in the two control groups (cerebral cortex target and cerebellar cortex target, $n = 3$ per group) underwent the surgical procedure, including cranial thinning and light exposure but were administered with saline only, and then, the mice were euthanized 24 h later for brain tissue collection

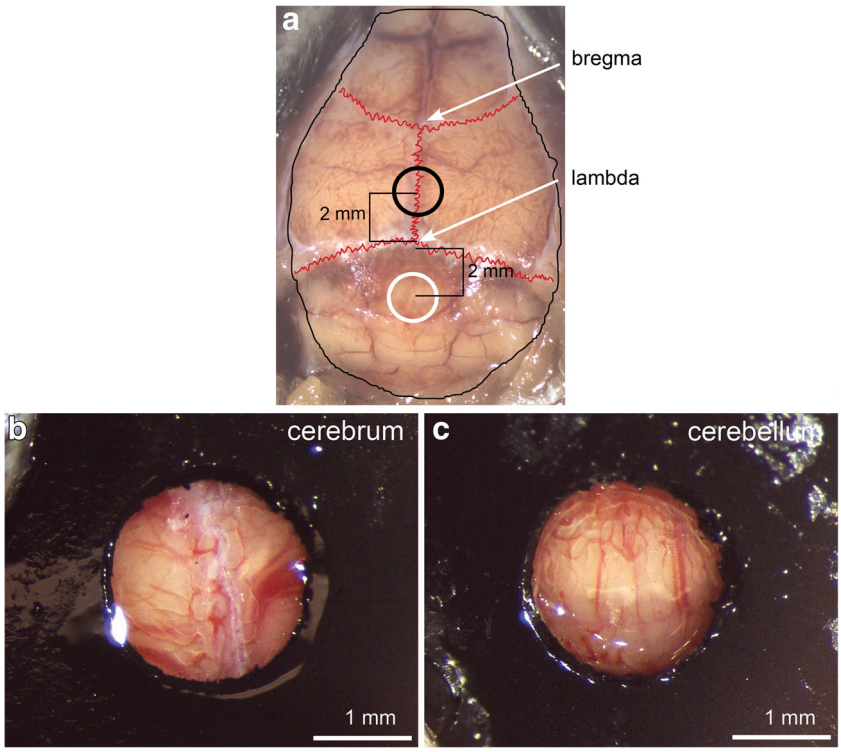

Fig. 1 Equivalent photothrombotic infarcts in the cerebral cortex and the cerebellar cortex were achieved by placing a mask with a fixed aperture over the skull to prevent stray light causing blood vessel occlusion outside of the target area. The 532 nm (green) laser used to illuminate the brain tissue was positioned at a fixed distance above this mask using a frame. **a** Schematic representation of the targeting of the two different brain regions of the photo-illumination. Images of the two target brain regions **b** cerebrum and **c** cerebellum, just prior to creating the photothrombotic lesions, illustrate the richly perfused brain tissue evident via cranial thinning. The aperture in the mask has a 2 mm diameter, providing ~ 3.5-mm^2 core infarct surface area

(1 day post-injury (DPI)). For the lesion groups, tissue collection was performed by euthanizing three mice at each census time point (2 h post-injury (HPI), and 1, 4, 7, 14, and 30 DPI), a total of 36 mice, which combined with the control groups, reflects the 42 mice used for the study.

Tissue Processing

For histological examination, mice were euthanised with Pentobarbital (100 mg/kg; 100 mg/ml intraperitoneal injection) and intracardially perfused with 10 ml of 0.01 M phosphate-buffered saline (PBS) followed by 10 ml of 4% paraformaldehyde (PFA) in 0.01 M phosphate buffer (pH 7.4). Whole brain was dissected and postfixed in the 4% PFA solution overnight at 4 °C. Tissue was cryoprotected in 10 and 30% sucrose in PBS overnight at 4 °C. Tissue was embedded in Tissue-Tek OCT compound (Sakura, USA) and sectioned coronally (50 μm thickness) using a cryostat (CM 1850, Leica Biosystems, Australia).

Immunofluorescence

Successive serial cerebral (1200 μm apart) and cerebellar sections (1000 μm apart) were probed with antibodies against neuronal nuclei (NeuN; Millipore, USA), glial fibrillary acidic protein (GFAP; Abcam, USA) and ionised calcium-binding adapter molecule 1 (Iba-1; Abcam, USA) to visualise neurons, astrocytes and microglia, respectively. In addition, cerebellar sections were also probed for Calbindin (Millipore, USA) to visualise Purkinje neurons. Sections were incubated with 15% normal serum and 1% TritonX-100 in 0.01 M PBS for 1 h at room temperature (RT) followed by overnight incubation with diluted polyclonal primary NeuN (1 in 2000), GFAP (1 in 1000), Iba-1 (1 in 500) and Calbindin (1 in 500) antibodies in 15% normal serum and 0.1% TritonX-100 in 0.01 M PBS at room temperature. The following day, sections were washed with PBS for 10, 20 and 40 min, incubated with diluted goat anti-rabbit Alexa Fluor 594 for NeuN, goat anti-chicken Alexa Fluor 647 for GFAP, goat anti-rabbit Alexa Fluor 488 for Calbindin (1 in 500 each) and rabbit anti-goat Alexa Fluor 568 for Iba-1 (1 in 1000) made in secondary antibody solution comprising 10% normal serum in 0.01 M PBS for 4 h at RT during which tissue was shielded from light. Sections were then washed with PBS for 10 and 20 min, followed by 10 min incubation with 4, 6-diamidino-2-phenyl indole (DAPI; Sigma-Aldrich, USA; 1:5000 in PBS) for 10 min at RT. Sections were washed in PBS for 10 and 40 min post-DAPI labelling and mounted on Superfrost® PLUS slides (Thermo Fisher Scientific, USA) using fluorescent mounting medium (Vector laboratories, USA). In all the aforementioned steps, normal goat serum was used for NeuN, GFAP and Calbindin antibodies and normal donkey serum for Iba-1 antibody.

Haematoxylin and Eosin (H&E) Staining

H&E histochemical labelling was performed on every twelfth cryosection (600 μm separation) of cerebral cortex infarct

regions and every tenth section (500 μm separation) for cerebellar cortex infarcts. The sections were mounted on Superfrost® PLUS slides and air-dried overnight, then rinsed in a series of xylol and decreasing concentrations of alcohol before incubation with haematoxylin. One percent acid alcohol and Scott's blue solutions were used to achieve contrast in the staining. Sections were incubated with counter stain eosin and dehydrated in increasing concentrations (70 and 100%) of ethanol followed by clearing in xylene, and then were cover slipped with DPX mounting medium.

Imaging and Infarct Analysis

Sections immunostained for NeuN, GFAP, Iba-1 and Calbindin were imaged using a fluorescent slide scanner (Aperio FL, Leica Biosystems) and converted to greyscale (Photoshop software, Adobe). Images for haematoxylin and eosin (H&E)-stained sections were captured using a bright field scanner (Aperio XT, Leica Biosystems) and utilised to draw contours around the circumference of the infarct in each section using ImageJ software (NIH, USA) to ascertain infarct area measurements. Total infarct volumes were calculated by summing of the infarct areas in each section multiplied by the interval between sections. Descriptive statistics, one-way analysis of variance (ANOVA) and two-way ANOVA, with confirmation of normally distributed data, were performed to determine significant differences among the treatment groups. Where data were not normally distributed, non-parametric (ranked) ANOVA was undertaken. Multiple pairwise comparisons were conducted using the Holm-Sidak method, and data are represented as mean ± standard error of mean (SEM). All descriptive and statistical analysis used Sigmaplot software (Systat, USA).

Results

Cellular Responses to Photothrombotic Lesion in the Cerebral Cortex

H&E staining and immunofluorescence were employed to visualise tissue integrity and cellular responses to photothrombotic lesions in the mouse cerebral cortex at 2 HPI, 1, 4, 7, 14, and 30 DPI. Control sections stained with H&E showed normal cerebral cyto-architecture (Fig. 2a). Immunofluorescence with NeuN revealed the healthy distribution of neurons in the cerebral cortex and hippocampus (Fig. 2b). Irradiation with green light resulted in a clear disruption of tissue integrity in the cerebral cortex at 2 HPI, as seen in the H&E-stained sections; however, the underlying hippocampal structure was not affected (Fig. 2e). NeuN immunostaining (Fig. 2f) showed clear loss of neurons compared to the control at 2 HPI. Both H&E and NeuN staining revealed an increase in tissue damage at 1 DPI (Fig. 2i, j), and this damage was greatest at 4 DPI, with a complete loss of neurons beyond the initial lesion site (Fig. 2m, n). Evidence of tissue shrinkage and scarring was visible at 7, 14 and 30 DPI (Fig. 2q, r, u, v, y, z) as the total area of tissue loss appeared smaller compared to 1 and 4 DPI.

To investigate cellular responses to ischaemia, immunofluorescence against astrocytes was performed with the GFAP antibody. The majority of the astrocytic staining was restricted to the outermost layer of the cortex and around the blood vessels in the control, 2 HPI and 1 DPI tissue (Fig. 2c, g, k). At 4 DPI, GFAP staining intensified around the lesion core (Fig. 2o) and continued around the lesion at 7, 14 and 30 DPI (Fig. 2s, w, aa) forming a barrier between the healthy and damaged tissue. Higher power imaging at 14 DPI (representative insert in Fig. 2w) revealed the reactive astrocytic phenotype encompassing the lesion site.

Iba-1 staining was used to visualise changes in microglial phenotype in response to the photothrombotic lesion. The control slice demonstrated an evenly distributed basal level of microglial Iba-1 staining. High magnification imaging revealed that majority of the microglia were of the quiescent ramified morphology, with few reactive/activated microglia (Fig. 2d). At 2 HPI, microglia were evenly distributed; however, activated/reactive microglia, evident as enlarged cell bodies with short or no processes, were the predominant phenotype in the injury zone (Fig. 2h). At 1 DPI, there was an increase in the presence of activated microglia (Fig. 2l) which further increased at 4 DPI, with a particularly high density of activated microglia now populated around the lesion (Fig. 2p). At 7 DPI, activated microglia had infiltrated the lesion site (Fig. 2t) and remained there at 14 and 30 DPI (Fig. 2x, ab, respectively). The higher magnification inserts further illustrate the sustained increase in the density of microglia staining following the lesion (Fig. 2a, x).

Cellular Responses to Photothrombotic Lesion in the Cerebellar Cortex

Cerebellar damage and lesion progression were visualised using the H&E staining in animals that underwent photothrombosis at 2 HPI, 1, 4, 7, 14 and 30 DPI. The cerebellar architecture, including the granule layer (GL) containing granule cells, and the molecular layer (ML) with the Purkinje neuron dendrites, were clearly distinguishable in the control tissue (Fig. 3a). The Purkinje layer (PL) located in between the GL and ML, containing Purkinje neuron somata, was not readily discernible in this staining. Damage to these layers was evident at 2 HPI at the site of irradiation (Fig. 3b). A stark increase in tissue damage was observed at 1 DPI (Fig. 3c), where regions of complete disruption of GL, PL and ML were evident at the site of irradiation of 1 DPI and 4 DPI (Fig. 3c, d). Tissue remodelling can be observed at 7 DPI where the infarct region was reduced (Fig. 3e) and this

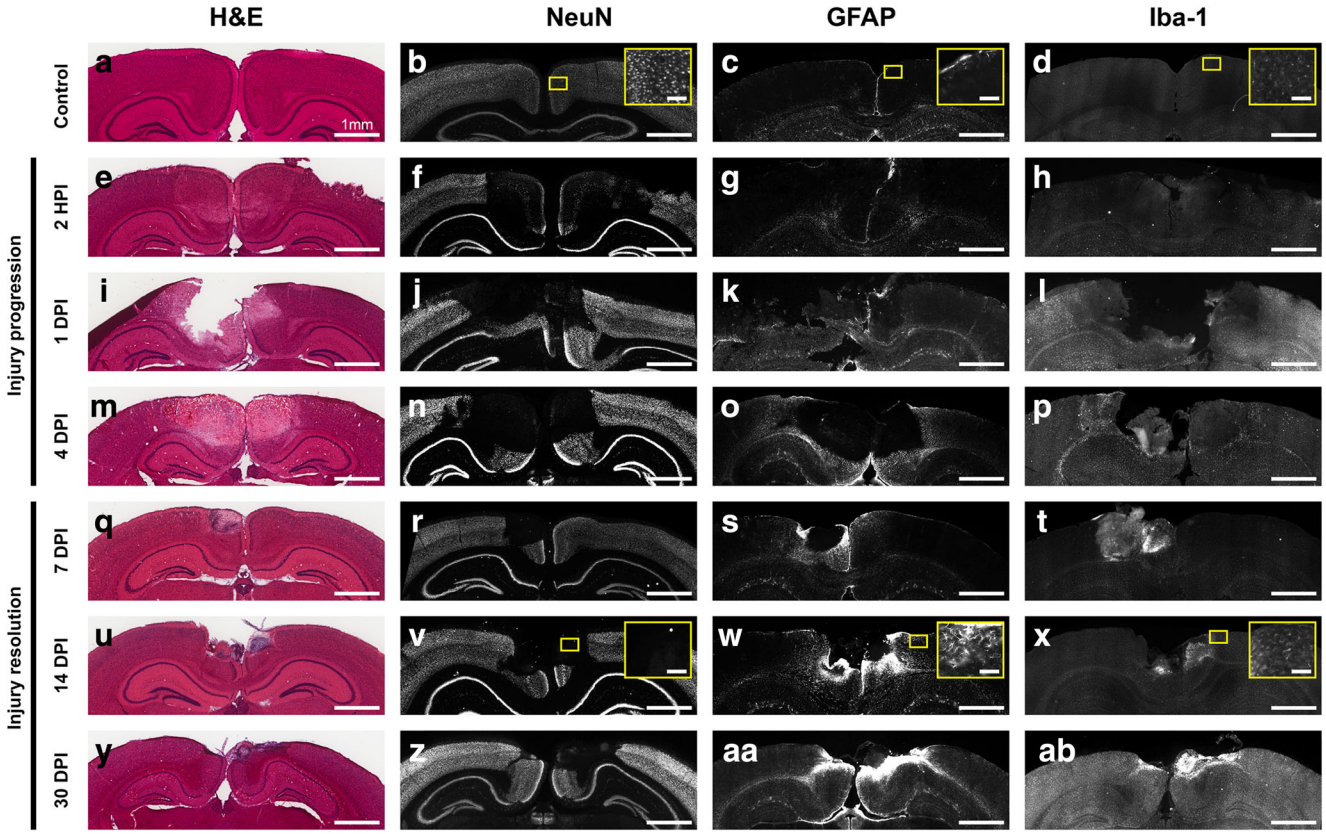

Fig. 2 Cellular responses to photothrombotic lesions in the mouse cerebral cortex out to 30 days post-injury (DPI). Representative haematoxylin and eosin (H&E) stained images from the following: photo-irradiation only control (no Rose Bengal dye) (**a**), mid-infarct 2 h post-injury (HPI) (**e**), 1 DPI (**i**), 4 DPI (**m**), 7 DPI (**q**), 14 DPI (**u**) and 30 DPI (**y**), highlight the expansion and remodelling of the ischaemic injury. Immunofluorescence was performed on serial sections with the neuronal nuclei (NeuN) antibody to label neurons, glial fibrillary acidic protein (GFAP) antibody to label astrocytes and ionised calcium-binding adapter molecule 1 (Iba-1) antibody to visualise microglia, from cryosections adjacent to the H&E sections. Tissue integrity in the infarct was particularly compromised at 1 DPI. Representative greyscale images illustrate neuronal labelling in control tissue (**b**) and the damage ensued at 2 HPI (**f**), 1 DPI (**j**), 4 DPI (**n**), 7 DPI (**r**), 14 DPI (**v**) and 30 DPI (**z**). Basal level of GFAP staining was observed in the representative greyscale image from control section (**c**), 2 HPI (**g**). Increased levels of GFAP staining indicated astrocytic activation at 1 DPI (**k**) and 4 DPI (**o**), with glial scar formation at 7 DPI (**s**), 14 DPI (**w**) and 30 DPI (**aa**) around the site of photothrombotic lesion. Iba-1 immunofluorescence exhibited ramified, quiescent microglia sparsely yet evenly distributed across the control section (**d**). A change in the morphology to a more reactive microglia phenotype was observed in 2 HPI (**h**) and 1 DPI (**i**) sections. At 4 DPI (**p**), the density of microglial staining further increased and the majority of the microglia surrounding the lesion site were of the activated phenotype. At 7 DPI (**t**), 14 DPI (**x**) and 30 DPI (**ab**), the phagocytic amoeboid shaped microglia had infiltrated the lesion site. High power images of NeuN, GFAP and Iba-1 enclosed in the yellow boxes for control and 14 DPI sections show detailed cell morphology (scale bar **b**–**d**, **f**–**h**, **j**–**l**, **n**–**p**, **r**–**t**, **v**–**x**, **z**–**ab** = 100 μm). The lesions were predominantly centred around the midline, but some laterality was evident across the rostro-caudal extent of a few of the cerebral cortex infarcts

is continued through 14 and 30 DPI, with evidence of tissue shrinkage (Fig. 3f, g).

NeuN immunostaining in the control tissue revealed the characteristically high neuronal density of the GL (Fig. 4a). Calbindin staining in the control tissue showed the Purkinje neuron somata in the PL and the associated dendrites in the ML (Fig. 4b). Both markers revealed loss of granule cells and Purkinje neurons at 2 HPI, indicated by reduction in NeuN and Calbindin staining, respectively (Fig. 4e, f). A complete loss of staining was observed at 1 DPI and 4 DPI suggesting loss of granule cells and Purkinje neurons at the site of irradiation (Fig. 4i, j, m, n). Tissue remodelling began at 7DPI and continued at 14 and 30 DPI, resulting in a reduced area of neuronal loss (Fig. 4q, r, u, v, y, z).

Immunofluorescence with the GFAP antibody showed the activation of astrocytes in response to the photothrombotic injury. Astrocytic labelling was observed around blood vessels in control tissue and at 2 HPI (Fig. 4c, g). An increase in GFAP expression was seen at 1 and 4 DPI (Fig. 4k, o). Dense recruitment of astrocytes was observed at the infarct border at 7 DPI (Fig. 4s), indicating glial scar formation, and this astrocytic scarring was maintained at 14 and 30 DPI (Fig. 4w, aa). Immunolabelling with Iba-1 antibody was again used to investigate microglial response to photothrombotic lesion. An evenly distributed level of microglial staining was observed in control tissue (Fig. 4d), and a reasonably similar staining intensity was observed at 2 HPI and 1 DPI (Fig. 4h, l). However, at 4 DPI, microglial staining began to intensify around the

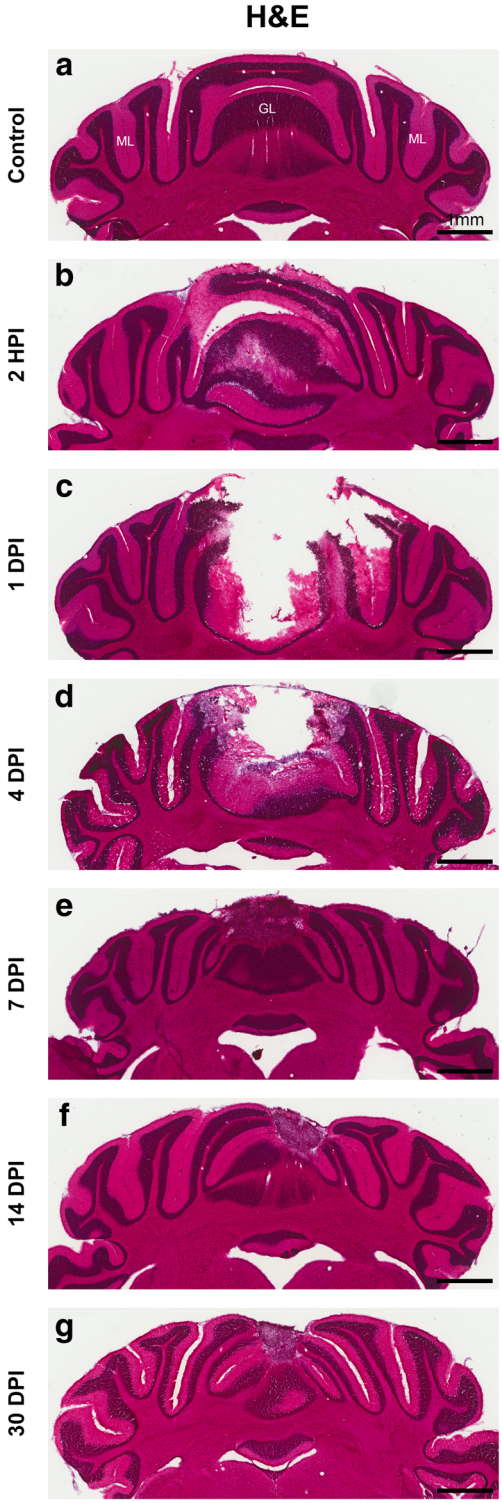

Fig. 3 Haematoxylin and eosin (H&E) staining of the mouse cerebellum following photothrombotic lesions. **a** Representative image of the photo-irradiation only control (no Rose Bengal dye) demonstrates the healthy granule layer (GL), containing granule cells and the healthy molecular layer (ML), containing the Purkinje neuron dendrites, devoid of injury. Representative mid-infarct cerebellar sections at 2 h post-injury (**b**), 1 day post-injury (DPI) (**c**), 4 DPI (**d**), 7 DPI (**e**), 14 DPI (**f**) and 30 DPI (**g**), illustrating injury expansion and tissue remodelling

infarct boundary, with the cells adopting an activated (circular) morphology (Fig. 4p). At 7, 14 and 30 DPI, amoeboid shaped reactive microglia had infiltrated into the lesion core at a high density, resulting in a more intense Iba-1 staining pattern (Fig. 4t, x, ab).

Quantitative Comparison of Photothrombotic Infarcts in the Cerebral Cortex and Cerebellum over Time

The sizes of the infarcts were calculated from the reconstructed injury zones in series of coronal cryosections stained with H&E. Figure 5 maps out the infarct volumes for the cerebral cortex (Fig. 5a) and cerebellum (Fig. 5b) across the different post-injury time points. The highest infarct volume in the cerebral cortex was observed at 4 DPI, followed by a steep decline in the infarct volumes at the subsequent time points due to tissue remodelling (Figs. 5a, 2). In comparison, in the cerebellum, infarct volumes expanded rapidly, to a maximum at 1 DPI (equivalent in size to the 4 DPI cerebral cortex lesion), and resolved more gradually during the 30-day census period (Figs. 3, 4 and 5b). For cerebral cortex, at 2 HPI, the infarct volume was 2.77 ± 0.76 mm^3 (Fig. 5a). This expanded to a maximum volume of 17.33 ± 3.98 mm^3 at 4 DPI (Fig. 5a) ($p = 0.002$, 2 HPI vs 4 DPI, one-way ANOVA). In contrast, the infarct volume in the cerebellum at 2 HPI was 7.20 ± 0.76 mm^3 (Fig. 5b) and reached a maximum of 18.85 ± 3.92 mm^3 at 1 DPI (Fig. 5b) ($p = 0.014$, 2 HPI vs 1 DPI, one-way ANOVA). There was an overall significant difference between the lesion volumes of the cerebral cortex and cerebellum across the time intervals ($p < 0.001$, two-way ANOVA on ranks; $n = 3$ for each brain region at each time point). The mean infarct volumes in the cerebellum were higher than the infarct volumes in the cerebral cortex at 2 HPI, 1 DPI, 7 DPI, 14 DPI and 30 DPI ($p = 0.029$, 0.002, 0.040, 0.034, 0.029, respectively; Holm–Sidak multiple comparisons). At 4 DPI, the mean infarct volumes in the cerebral cortex and cerebellum were not significantly different ($p = 0.324$; power of performed test with alpha = 0.0500, for time point × region: 0.359).

Figure 6 provides spatiotemporal profiles of the lesions in the two brain regions, by reporting the mean cross-sectional areas of infarcted tissue at different rostro-caudal locations through the lesions. This shows that the infarct expansion is proportionately greater in the dorso-ventral plane at the centre of the infarcts, relative to rostro-caudal spread, for both cerebral cortex (comparing 2 HPI with 4 DPI) and cerebellum (comparing 2 HPI with 1 DPI). For cerebral cortex, the rostro-caudal spread of the infarcts expanded by ~ 1.8 mm to a maximum of 4.2 mm (75% increase) (Fig. 6a); with the largest change in cross-sectional area occurring at the midpoint of the lesion, where the mean increased from ~ 2 to ~ 6 mm^2 (200% increase). The tissue injury in the cerebellum at 2 HPI spanned 4 mm rostro-caudally, with the mean cross-sectional area of infarct within these sections being ~ 2 mm^2

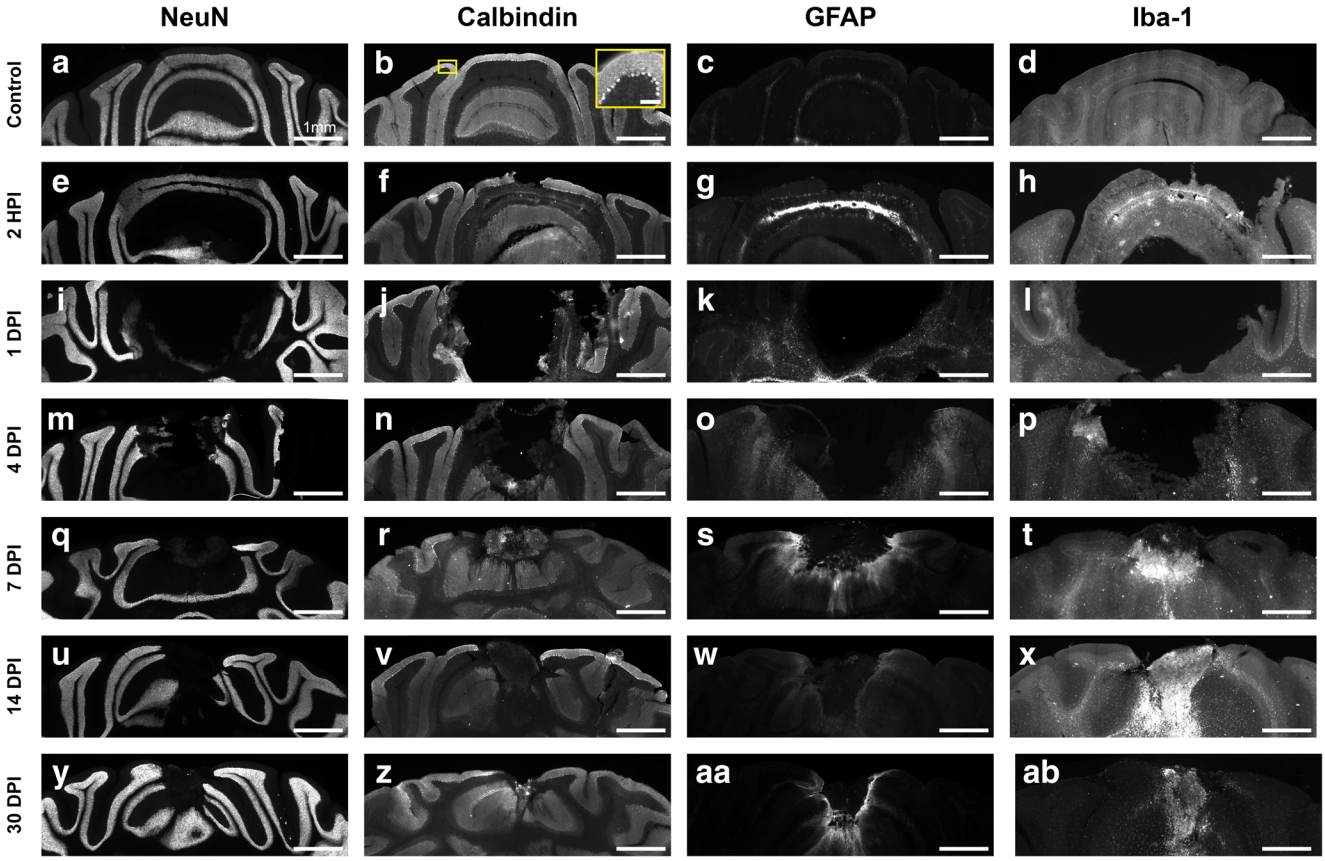

Fig. 4 Characterisation of cellular responses to photothrombotic lesions in the mouse cerebellum. Adjacent serial sections were stained with neuronal nuclei (NeuN) and Calbindin antibody to visualise granule cells and Purkinje neurons, respectively. Glial fibrillary acidic protein (GFAP) and ionised calcium-binding adapter molecule 1 (Iba-1) antibodies were employed to visualise changes in astrocyte and microglia density and morphologies, respectively. Representative mid-infarct greyscale images of NeuN immunofluorescence sections: photo-irradiation only control (no Rose Bengal dye) (**a**), 2 h post-injury (HPI) (**e**), 1 day post-injury (DPI) (**i**), 4 DPI (**m**), 7 DPI (**q**), 14 DPI (**u**) and 30 DPI (**y**) and corresponding Calbindin immunofluorescence sections from the same infarct regions: control (**b**), 2 HPI (**f**), 1 DPI (**j**), 4 DPI (**n**), 7 DPI (**r**), 14 DPI (**v**) and 30 DPI (**z**) indicate loss of granule cells and Purkinje neurons. Representative greyscale images indicate a basal level of GFAP staining in the control (**c**) and 2 HPI (**g**) cerebellar sections. Increase in GFAP levels was evident at 1 DPI (**k**), 4 DPI (**o**) and the formation of scar tissue was observed at 7 DPI (**s**), 14 DPI (**w**) and 30 DPI (**aa**). **d** Representative greyscale images of immunofluorescence of microglia labelled with the Iba-1 antibody shows a low level of staining in the control section with a low density of ramified microglia evenly distributed through the tissue. **h** At 2 HPI, the ramified microglia were observed at a higher intensity as compared to control. At 1 DPI, the majority of the microglia appeared to be of the activated morphology (**l**) and at 4 DPI these activated microglia were more densely populated around the lesion area (**p**). At 7 DPI, the microglia had infiltrated the lesion site (**t**) and remained there at 14 DPI (**x**) and 30 DPI (**ab**)

(Fig. 6b). There was no rostro-caudal expansion of the cerebellar infarcts at 1 DPI, but the cross-sectional area of injury increased to a maximum of ~ 9 mm^2 at the mid-point of the lesion (~ 350% increase) (Fig. 6b).

Discussion

In this study, we have established and compared the spatio-temporal profiles of the expansion and resolution of photothrombotic lesions in the cerebral cortex and the cerebellum, along with characterisation of the neuronal damage and glial responses to the focal ischaemic injury. Equivalent brain microvascular occlusions in the cerebellar and cerebral cortices were achieved by delivering the same flux of 532 nm laser light for photothrombotic activation via the same masked aperture and for the same fixed time period. This was evident from the visualisation of the initial thrombosis at ~ 3.5 mm^2 on the brain surfaces, when the mask was removed. Infarct progression was consistently greater in the cerebellum from as early as 2 HPI, and the larger cerebellar infarct areas were maintained across the 30-day study period. The peak of the injury in the cerebellum was earlier than that in the cerebrum (1 DPI), indicating a faster expansion of the ischaemic penumbra in the cerebellar cortex. The controls matched the skull thinning and photonic excitation, but the Rose Bengal photosensitising dye was substituted for normal saline carrier in the tail vein injections. The lack of injury markers in the controls indicates that the laser light alone, or the thinning procedure, did not contribute to the injury response.

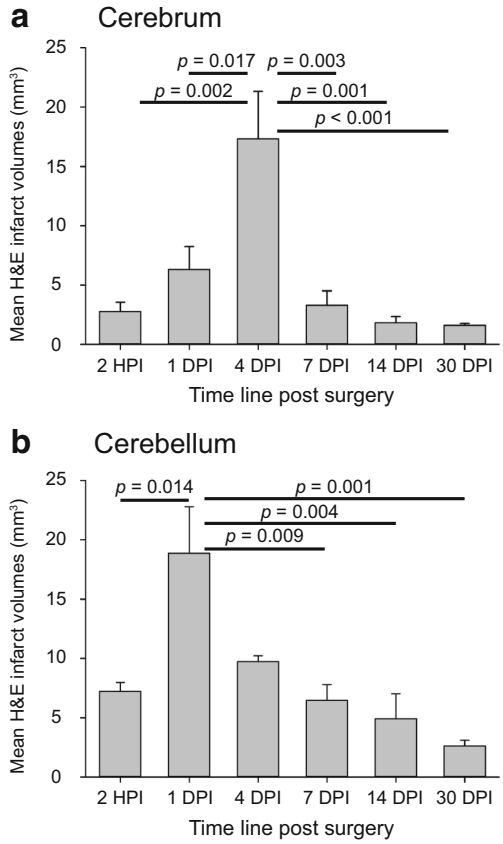

Fig. 5 Assessment of infarct volumes of the mouse cerebral cortex and cerebellum following photothrombotic lesions. **a** Cerebral infarct volumes at 2 h post-injury (HPI), 1 day post-injury (DPI), 4 DPI, 7 DPI, 14 DPI and 30 DPI. Infarct volume at 4 DPI in the cerebral cortex was higher than at any other time point. **b** In the cerebellum, the maximal infarct volume was observed at 1 DPI. $n = 3$ per time point for both brain regions; one-way ANOVA, Holm-Sidak post hoc

A primary assumption of the study is that the thrombosis generated by photo-illumination of the Rose Bengal dye in the blood vessels is equivalent for the two targeted brain regions. The superficial blood vessels are shown in Fig. 1 and are evidently comparable across the two sites; however, occlusion of the underlying microvessels are the primary substrate of the acute photothrombotic infarct. These microvessels may have diameters as small as ~8 μm and are at a consistently high density in the brain, forming a complex with pericytes and astrocytes to establish the neurovascular unit that ensures oxygen and nutrient supply to the immediately adjacent neurons and glia [27, 28]. Consistent with this, masking around the field of illumination was effective in achieving consistency in the blood flow occlusion both between experiments and across the two target brain regions.

While the progression of the infarct and the ensuing neuronal damage in the cerebral cortex following photothrombotic lesions in rodents has been previously studied [16, 20, 26, 29, 30], the inherent utility of this approach to provide highly reproducible, discrete thrombotic infarcts for direct comparison of ischaemic injury in different brain regions has not been exploited. In the cerebellum, the infarct volume was found to be greatest at 1 DPI with subsequent tissue remodelling and glial responses progressively resolving the injury from 7 DPI onwards [30, 31]. This was different to the infarct progression in the cerebral cortex, as those lesions did not reach peak expansion until 4 DPI, suggesting that the complex processes underlying ischaemic brain injury [18] contribute differentially to the progression of the injury in these two brain regions. There are a number of potential molecular mechanisms that may be responsible for this different rate of injury expansion. For example, ischaemia in cortical neurons leads to glutamatergic excitotoxic neuronal injury triggered via Na^+ and Ca^{2+} loading of neurons, largely through the *N*-methyl-D-aspartate (NMDA) receptor [32, 33]. Adult Purkinje neurons, however, do not express functional NMDA receptors [34], and excitotoxic neuronal injury in Purkinje neurons likely involves Ca^{2+} entry through the alpha-amino-3-hydroxy-5-methyl-4-

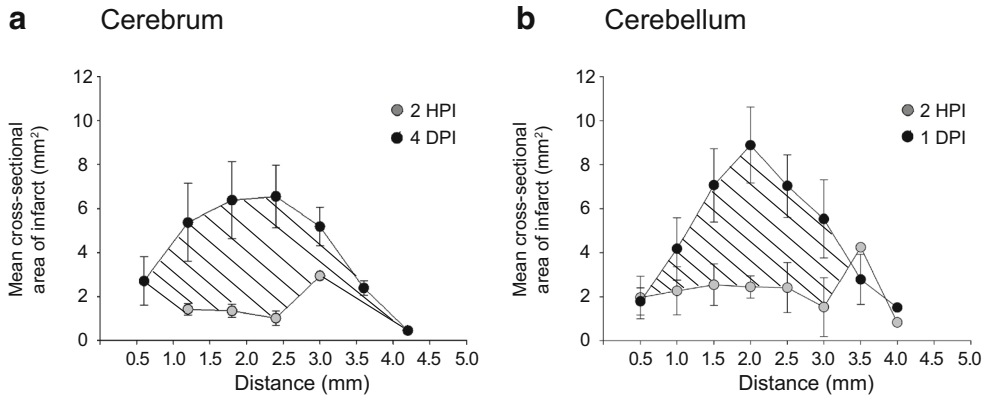

Fig. 6 Maximum expansion of the photothrombotic lesion in the cerebral cortex and cerebellum was seen at different time points. The mean cross-sectional infarct area for the rostro caudal series of haematoxylin and eosin stained cerebral sections at 2 h post-injury (2 HPI, grey circles) and 4 days post-injury (4 DPI, black circles; **a**) and cerebellar sections at 2 HPI (grey circles) and 1 DPI (black circles; **b**), demonstrated the expansion of the infarct area over time (shaded regions). Note the expansion of the penumbra from the central regions of both brain regions over time. $n = 3$ infarcts for each time point for each brain region

isoxazolepropionic acid (AMPA) receptor and Kainate receptor-type ionotropic glutamate receptors [35–38]. This vulnerability reflects the extensive glutamatergic parallel and climbing fibre inputs [39], combined with an insufficiency in glutamate reuptake following ischaemia [40, 41]. The more prominent white matter tracts in the cerebellum may also contribute to a differential ischaemic injury response [42].

The increased vulnerability of Purkinje neurons to undergo the necrotic form of cell death, which is more rapid than apoptotic cell death, has been linked to post-synaptic class I metabotropic glutamate receptor (mGluRI; either mGluR1 or mGluR5)-mediated signal transduction in an incomplete global ischaemia canine model [43]. Such mGluRI-driven glutamate excitotoxicity in the cerebellar Purkinje neurons is very likely to be mediated by canonical transient receptor potential (TRPC) ion channels. In mice, TRPC3 is the exclusive non-selective cation channel effector of mGluR1 signalling (via $G_{\alpha q}$–phospholipase C_{β}, –phosphoinositol bisphosphate–diacylglycerol) and is responsible for the slow excitatory post-synaptic potential component of parallel fibre synaptic transmission [44]. Additionally, across rodent species, Purkinje neurons dominantly express a truncated isoform of the TRPC3 gene, which lacks a regulatory domain providing negative feedback inhibition of the channel in the presence of high cytosolic Ca^{2+}, which would further exacerbate the contribution of these ion channels to depolarization and Ca^{2+} loading in the Purkinje neurons following an ischaemic excitotoxic insult [45, 46]. This 'Ca^{2+}-feedback uncoupled' splice variant of the TRPC3 ion channel is also present in the human cerebellum [45], and these channels, along with related mGluRI-linked TRPC channel subtypes (TRPC1, C6, C7), show differential expression in the cerebellum and cerebral cortices (Allen Mouse Brain Atlas: http://mouse.brain-map.org/). Overall, this potential enhanced vulnerability of cerebellar Purkinje neurons to excessive mGluR-mediated TRPC cation channel activation with ischemia may be a primary driver for the enhanced vulnerability of the cerebellum established here.

Despite a different rate of brain tissue injury progression, and resolution, in cerebellum and cerebral cortex, the glial spatiotemporal response profiles were conserved across the two brain regions. Astrocytic responses and microglia activation occurred jointly with injury in both regions, astrocytic invasion of the infarct was tied to the initiation and progression of the tissue remodelling, and a resident microglia population was also installed and remained even once resolution of neuronal damage had stabilised at 30 DPI. These glial responses match those characterised in previous photothrombotic lesion studies [31, 47]. GFAP immunolabelled astrocyte staining intensity and changes in the astrocytic morphology to the reactive form occurred around 7 DPI in both the brain regions. Enlarged reactive astrocytes encompassing the infarct site resulted in formation of a barrier between healthy and injured tissue at 7, 14 and 30 DPI. The role for the astrocytes in remodelling brain tissue with stroke has been established using GFAP knock out mice, where loss of expression of this astrocyte-specific protein resulted in increased cerebral cortex infarct volumes [48, 49].

Microglia, the principal innate immune cells of the brain, were identified by Iba-1 immunolabelling in this study. In cerebral cortex, the activation of microglia at the site of lesion and changes in the morphological phenotype of microglia was consistent with previous studies involving MCAO focal ischaemia [50] and photothrombotic lesions [21, 30]. Activated microglia were observed at 1 DPI in both the cerebral cortex and cerebellum as a result of neuronal damage [51], demonstrating enlarged soma size and stout processes compared to the quiescent or non-activated microglia phenotype in the control. A dense population of activated microglia at the vicinity of the infarct could be a result of proliferation of local microglia [52], or by migration of more distal microglia via ATP signalling [53]. It has been demonstrated in cortical inflammation models that the activated microglia are able to migrate to the site of lesion and strip the axosomatic synapses, improving neuronal survival [52, 54]. Studies of organotypic hippocampal cultures demonstrated the microglia migrated and surrounded the neurons at the site of injury to confer neuroprotection from ischaemic insult within 4 h of the injury [55]. Hence, at 7 DPI, activated microglia that infiltrated the lesion site completely in both the regions likely contributed to clearance of cellular debris, overall resolution of the photothrombotic lesion and reduced infarct volume.

The photothrombotic lesion method employed in this study is ideal for the comparison of brain injury at the cellular level across brain regions, as the lesions are constrained to a consistent superficial level of the cortex (due to limits to the penetration of the photo-illumination that activates the Rose Bengal dye in the microvessels). This essentially dissects the cellular response of strokes, but does not address the variance and complexity of stroke injury evident in the clinic due to broad and highly varying occlusion and reperfusion of the brain associated with the major vessels coupled to the circle of Willis and the medial cerebral arteries, which dominate thrombotic or haemorrhagic strokes, as described previously [56, 57].

In conclusion, this study established that photothrombosis is an effective model for delivery of focal ischaemic injury to the cerebellum, as well as the cerebral cortex. The injuries produced in this model were quantifiable, reproducible, spatio-temporally constrained, produced a penumbra and elicited glial responses and therefore validated our aperture-regulated photothrombotic infarct protocol for direct comparison of acute focal ischaemic brain injury in the mouse between the cerebellar cortex and cerebral cortex. The data resolved the faster progression and greater vulnerability of cerebellar ischaemic injury to the same photothrombotic challenge, which suggests that different and more excitotoxic

transduction cascades are inherent within the cerebellum. These findings further indicate that the mouse model is relevant to the evidential clinical vulnerability of patients with posterior circulation strokes and highlight the need for verifying therapeutic efficacy in multiple brain regions during drug development studies.

Acknowledgements Funded by UNSW Sydney 'Goldstar' awards and philanthropic support from the Stephen Fairfax Bequest to the UNSW Foundation.

Author's Contribution Conceptualization, G.D.H. A.J.C., N.G. and J.P.; methodology, G.D.H. A.J.C., N.G. and J.P.; investigation, N.G., J.P. and G.D.H.; writing–original draft, N.G., J.P. and G.D.H.; writing–review and editing, N.G., J.P., G.D.H., A.J.C., J.M.P., A.J.M., A.V.K; funding acquisition, G.D.H., A.J.C., J.M.P., A.J.M., A.V.K..

Compliance with Ethical Standards

All experiments were approved by the UNSW Sydney Animal Care and Ethics Committee.

Conflict of Interest The authors declare that they have no conflict of interest.

Ethical Approval All animal experiments were conducted in accordance with the UNSW Sydney Animal Care and Ethics Committee.

References

1. Jauch EC, Saver JL, Adams HP Jr, Bruno A, Connors JJ, Demaerschalk BM, et al. American Heart Association stroke council; council on cardiovascular nursing; council on peripheral vascular disease; council on clinical cardiology. Guidelines for the early management of patients with acute ischemic stroke: a guideline for healthcare professionals from the American Heart Association/American Stroke Association. Stroke. 2013;44:870–947.
2. Fonarow GC, Smith EE, Saver JL, Reeves MJ, Bhatt DL, Grau-Sepulveda MV, et al. Timeliness of tissue-type plasminogen activator therapy in acute ischemic stroke: patient characteristics, hospital factors, and outcomes associated with door-to-needle times within 60 minutes. Circulation. 2011;123:750–8.
3. Nogueira RG, Jadhav AP, Haussen DC, Bonafe A, Budzik RF, Bhuva P, et al. 6 to 24 hours after stroke with a mismatch between deficit and infarct. N Engl J Med. 2017;378:11–21. https://doi.org/10.1056/NEJMoa1706442.
4. Khatri P, Abruzzo T, Yeatts SD, Nichols C, Broderick JP, Tomsick TA, et al. Good clinical outcome after ischemic stroke with successful revascularization is time-dependent. Neurology. 2009;73:1066–72.
5. Quillinan N, Grewal H, Deng G, Shimizu K, Yonchek JC, Strnad F, et al. Region-specific role for GluN2B-containing NMDA receptors in injury to Purkinje cells and CA1 neurons following global cerebral ischemia. Neuroscience. 2015;284:555–65.
6. Horn M, Schlote W. Delayed neuronal death and delayed neuronal recovery in the human brain following global ischemia. Acta Neuropathol. 1992;85:79–87.
7. Sato M, Chang E, Igarashi T, Noble LJ. Neuronal injury and loss after traumatic brain injury: time course and regional variability. Brain Res. 2001;917:45–54.
8. Slemmer JE, De Zeeuw CI, Weber JT. Don't get too excited: mechanisms of glutamate-mediated Purkinje cell death. Prog Brain Res. 2005;148:367–90.
9. Macdonell RA, Kalnins RM, Donnan GA. Cerebellar infarction: natural history, prognosis, and pathology. Stroke. 1987;18:849–55.
10. Ng ZX, Yang WR, Seet E, Koh KM, Teo KJ, Low SW, et al. Cerebellar strokes: a clinical outcome review of 79 cases. Singap Med J. 2015;56:145–9.
11. Woitzik J, Schneider UC, Thome C, Schroeck H, Schilling L. Comparison of different intravascular thread occlusion models for experimental stroke in rats. J Neurosci Methods. 2006;151:224–31.
12. Hata R, Mies G, Wiessner C, Fritze K, Hesselbarth D, Brinker G, et al. A reproducible model of middle cerebral artery occlusion in mice: hemodynamic, biochemical, and magnetic resonance imaging. J Cereb Blood Flow Metab. 1998;18:367–75.
13. Ansar S, Chatzikonstantinou E, Wistuba-Schier A, Mirau-Weber S, Fatar M, Hennerici MG, et al. Characterization of a new model of thromboembolic stroke in C57 black/6J mice. Transl Stroke Res. 2014;5:526–33.
14. Orset C, Macrez R, Young AR, Panthou D, Angles-Cano E, Maubert E, et al. Mouse model of in situ thromboembolic stroke and reperfusion. Stroke. 2007;38:2771–8.
15. Ansari S, Azari H, Caldwell KJ, Regenhardt RW, Hedna VS, Waters MF, Hoh BL, Mecca AP. Endothelin-1 induced middle cerebral artery occlusion model for ischemic stroke with laser Doppler flowmetry guidance in rat. J Vis Exp. 2013;72.
16. Labat-Gest V, Tomasi S. Photothrombotic ischemia: a minimally invasive and reproducible photochemical cortical lesion model for mouse stroke studies. J Vis Exp. 2013;(76). https://doi.org/10.3791/50370.
17. Yao H, Sugimori H, Fukuda K, Takada J, Ooboshi H, Kitazono T, et al. Photothrombotic middle cerebral artery occlusion and reperfusion laser system in spontaneously hypertensive rats. Stroke. 2003;34:2716–21.
18. Sommer CJ. Ischemic stroke: experimental models and reality. Acta Neuropathol. 2017;133:245–61.
19. Abeysinghe HC, Bokhari L, Dusting GJ, Roulston CL. Brain remodelling following endothelin-1 induced stroke in conscious rats. PLoS One. 2014;9:e97007.
20. Watson BD, Dietrich WD, Busto R, Wachtel MS, Ginsberg MD. Induction of reproducible brain infarction by photochemically initiated thrombosis. Ann Neurol. 1985;17:497–504.
21. Schroeter M, Jander S, Stoll G. Non-invasive induction of focal cerebral ischemia in mice by photothrombosis of cortical microvessels: characterization of inflammatory responses. J Neurosci Methods. 2002;117:43–9.
22. Lee JK, Park MS, Kim YS, Moon KS, Joo SP, Kim TS, et al. Photochemically induced cerebral ischemia in a mouse model. Surg Neurol. 2007;67:620–5.
23. Fluri F, Schuhmann MK, Kleinschnitz C. Animal models of ischemic stroke and their application in clinical research. Drug Des Dev Ther. 2015;9:3445–54.
24. Henninger N, Eberius KH, Sicard KM, Kollmar R, Sommer C, Schwab S, et al. A new model of thromboembolic stroke in the posterior circulation of the rat. J Neurosci Methods. 2006;156:1–9.
25. Sekiguchi M, Takagi K, Takagi N, Date I, Takeo S, Tanaka O, et al. Time course and sequence of pathological changes in the cerebellum of microsphere-embolized rats. Exp Neurol. 2005;191:266–75.
26. Talley Watts L, Zheng W, Garling RJ, Frohlich VC, Rose LJD. Bengal photothrombosis by confocal optical imaging *in vivo*: a model of single vessel stroke. J Vis Exp. 2015;100:e52794.
27. Xiong B, Li A, Lou Y, Chen S, Long B, Peng J, et al. Precise cerebral vascular atlas in stereotaxic coordinates of whole mouse brain. Front Neuroanat. 2017;11:128.

28. Zhang JH, Badaut J, Tang J, Obenaus A, Hartman R, Pearce WJ. The vascular neural network–a new paradigm in stroke pathophysiology. Nat Rev Neurol. 2012;8:711–6.
29. Pevsner PH, Eichenbaum JW, Miller DC, Pivawer G, Eichenbaum KD, Stern A, et al. A photothrombotic model of small early ischemic infarcts in the rat brain with histologic and MRI correlation. J Pharmacol Toxicol Methods. 2001;45:227–33.
30. Li H, Zhang N, Lin HY, Yu Y, Cai QY, Ma L, et al. Histological, cellular and behavioral assessments of stroke outcomes after photothrombosis-induced ischemia in adult mice. BMC Neurosci. 2014;15:58.
31. Nowicka D, Rogozinska K, Aleksy M, Witte OW, Spatiotemporal S-KJ. Dynamics of astroglial and microglial responses after photothrombotic stroke in the rat brain. Acta Neurobiol Exp. 2008;68:155–68.
32. Centeno C, Repici M, Chatton JY, Riederer BM, Bonny C, Nicod P, et al. Role of the JNK pathway in NMDA-mediated excitotoxicity of cortical neurons. Cell Death Differ. 2007;14:240–53.
33. Goldberg MP, Weiss JH, Pham PC, Choi DW. N-methyl-D-aspartate receptors mediate hypoxic neuronal injury in cortical culture. J Pharmacol Exp Ther. 1987;243:784–91.
34. Audinat E, Knopfel T, Gahwiler BH. Responses to excitatory amino acids of Purkinje cells' and neurones of the deep nuclei in cerebellar slice cultures. J Physiol. 1990;430:297–313.
35. Brorson JR, Manzolillo PA, Miller RJ. Ca^{2+} entry via AMPA/KA receptors and excitotoxicity in cultured cerebellar Purkinje cells. J Neurosci. 1994;14:187–97.
36. Brorson JR, Manzolillo PA, Gibbons SJ, Miller RJ. AMPA receptor desensitization predicts the selective vulnerability of cerebellar Purkinje cells to excitotoxicity. J Neurosci. 1995;15:4515–24.
37. Brasko J, Rai P, Sabol MK, Patrikios P, Ross DT. The AMPA antagonist NBQX provides partial protection of rat cerebellar Purkinje cells after cardiac arrest and resuscitation. Brain Res. 1995;699:133–8.
38. Craig AJ, Housley GD, Fath T. Modeling excitotoxic ischemic brain injury of cerebellar Purkinje neurons by intravital and in vitro multi-photon laser scanning microscopy. In: Bakota L, Brandt R, editors. Laser scanning microscopy and quantitative image analysis of neuronal tissue. New York: Springer; 2014. p. 105–27.
39. O'hearn E, Molliver ME. The olivocerebellar projection mediates ibogaine-induced degeneration of Purkinje cells: a model of indirect, trans-synaptic excitotoxicity. J Neurosci. 1997;17:8828–41.
40. Welsh JP, Yuen G, Placantonakis DG. Vu TQ, Haiss F, O'hearn E, Molliver ME, Aicher SA. Why do Purkinje cells die so easily after global brain ischemia? Aldolase C, EAAT4, and the cerebellar contribution to posthypoxic myoclonus. Adv Neurol. 2002;89:331–59.
41. Yamashita A, Makita K, Kuroiwa T, Tanaka K. Glutamate transporters GLAST and EAAT4 regulate postischemic Purkinje cell death: an in vivo study using a cardiac arrest model in mice lacking GLAST or EAAT4. Neurosci Res. 2006;55:264–70.
42. Bristow MS, Simon JE, Brown RA, Eliasziw M, Hill MD, Coutts SB, et al. MR perfusion and diffusion in acute ischemic stroke: human gray and white matter have different thresholds for infarction. J Cereb Blood Flow Metab. 2005;25:1280–7.
43. Martin LJ, Sieber FE, Traystman RJ. Apoptosis and necrosis occur in separate neuronal populations in hippocampus and cerebellum after ischemia and are associated with differential alterations in metabotropic glutamate receptor signaling pathways. J Cereb Blood Flow Metab. 2000;20:153–67.
44. Hartmann J, Henning HA, Konnerth A. mGluR1/TRPC3-mediated synaptic transmission and calcium signaling in mammalian central neurons. Cold Spring Harb Perspect Biol. 2011;3(4). https://doi.org/10.1101/cshperspect.a006726.
45. Kim Y, Wong AC, Power JM, Tadros SF, Klugmann M, Moorhouse AJ, et al. Alternative splicing of the TRPC3 ion channel calmodulin/IP3 receptor-binding domain in the hindbrain enhances cation flux. J Neurosci. 2012;32:11414–23.
46. Zheng F, Phelan KD. The role of canonical transient receptor potential channels in seizure and excitotoxicity. Cell. 2014;3:288–303.
47. Patience MJ, Zouikr I, Jones K, Clarkson AN, Isgaard J, Johnson SJ, et al. Photothrombotic stroke induces persistent ipsilateral and contralateral astrogliosis in key cognitive control nuclei. Neurochem Res. 2015;40:362–71.
48. Li L, Lundkvist A, Andersson D, Wilhelmsson U, Nagai N, Pardo AC, et al. Protective role of reactive astrocytes in brain ischemia. J Cereb Blood Flow Metab. 2008;28:468–81.
49. Liu Z, Li Y, Cui Y, Roberts C, Lu M, Wilhelmsson U, et al. Beneficial effects of gfap/vimentin reactive astrocytes for axonal remodeling and motor behavioral recovery in mice after stroke. Glia. 2014;62:2022–33.
50. Ito D, Tanaka K, Suzuki S, Dembo T, Fukuuchi Y. Enhanced expression of Iba1, ionized calcium-binding adapter molecule 1, after transient focal cerebral ischemia in rat brain. Stroke. 2001;32:1208–15.
51. Streit WJ. Microglial response to brain injury: a brief synopsis. Toxicol Pathol. 2000;28:28–30.
52. Li T, Pang S, Yu Y, Wu X, Guo J, Zhang S. Proliferation of parenchymal microglia is the main source of microgliosis after ischaemic stroke. Brain. 2013;136:3578–88.
53. Davalos D, Grutzendler J, Yang G, Kim JV, Zuo Y, Jung S, et al. ATP mediates rapid microglial response to local brain injury in vivo. Nat Neurosci. 2005;8:752–8.
54. Trapp BD, Wujek JR, Criste GA, Jalabi W, Yin X, Kidd GJ, et al. Evidence for synaptic stripping by cortical microglia. Glia. 2007;55:360–8.
55. Neumann J, Gunzer M, Gutzeit HO, Ullrich O, Reymann KG, Dinkel K. Microglia provide neuroprotection after ischemia. FASEB J. 2006;20:714–6.
56. Howells DW, Porritt MJ, Rewell SS, O'collins V, Sena ES, Van Der Worp HB, et al. Different strokes for different folks: the rich diversity of animal models of focal cerebral ischemia. J Cereb Blood Flow Metab. 2010;30:1412–31.
57. Traystman RJ. Animal models of focal and global cerebral ischemia. ILAR J. 2003;44:85–95.